Once $\tilde{a}$ and $\tilde{b}$ have been computed it can be shown by direct expansion that (46) is equivalent to the following recursive algorithm.

1) **Initialization**

$$\alpha_0 = 0, \tilde{a}_1 \rightarrow \tilde{a}_1 + Ad_{f_{0,1}^{-1}} \dot{V}_0. \tag{55}$$

2) **Forward recursion: for $k = 1$ to n do**

$$\alpha_k = Ad_{f_{k-1,k}^{-1}} \alpha_{k-1} + \tilde{a}_k \tag{56}$$

$$\overline{\alpha}_k = D_k \alpha_k + \tilde{b}_k. \tag{57}$$

3) **Initialization**

$$P_{n+1} = 0, \overline{\alpha}_n \rightarrow \overline{\alpha}_n + Ad^*_{f_{n,n+1}^{-1}} f_t. \tag{58}$$

4) **Backward recursion: for $k = n$ to 1 do**

$$P_k = Ad^*_{f_{k,k+1}^{-1}} P_{k+1} + \overline{\alpha}_k \tag{59}$$

$$\hat{P}_k = A_k^T P_k \tag{60}$$

$$\hat{\tau}_k = \tau_k - \hat{P}_k. \tag{61}$$

Once $\hat{\tau}$ has been computed it can be shown by direct expansion that (45) is equivalent to the following recursive algorithm.

1) **Initialization**

$$\hat{z}_{n+1} = 0, \hat{\tau}_{n+1} = 0. \tag{62}$$

2) **Backward recursion: for $k = n$ to 1 do**

$$\hat{z}_k = \overline{Y}_{k,k+1} \hat{z}_{k+1} + \overline{\Pi}_{k,k+1} \hat{\tau}_{k+1} \tag{63}$$

$$c_k = \hat{\tau}_k - A_k^T \hat{z}_k \tag{64}$$

$$\hat{c}_k = \Omega_k^{-1} c_k. \tag{65}$$

3) **Initialization**

$$\lambda_0 = 0. \tag{66}$$

4) **Forward recursion: for $k = 1$ to n do**

$$\lambda_k = \overline{Y}^T_{k-1,k} \lambda_{k-1} + A_k \hat{c}_k \tag{67}$$

$$\ddot{q}_k = \hat{c}_k - \overline{\Pi}^T_{k-1,k} \lambda_{k-1}. \tag{68}$$

Here

$$\overline{Y}_{k,k+1} = \overline{X}^T_{k+1,k} = Ad^*_{f_{k,k+1}^{-1}} \left(I - \frac{\hat{\overline{J}}_{k+1} A_{k+1} A_{k+1}^T}{A_{k+1}^T \hat{\overline{J}}_{k+1} A_{k+1}} \right)$$

and

$$\overline{\Pi}_{k,k+1} = \frac{Ad^*_{f_{k,k+1}^{-1}} \hat{\overline{J}}_{k+1} A_{k+1}}{A_{k+1}^T \hat{\overline{J}}_{k+1} A_{k+1}}.$$

VII. Conclusion

In this article, we have presented a unified coordinate-invariant formulation of the dynamics of multibody open chain manipulators based on standard concepts from geometry and mechanics. One of the major benefits of our geometric formulation is that it provides a single unified framework to express ideas originally introduced by Silver, Featherstone and Rodriguez *et al.* in a clean, concise, and coordinate-invariant manner. We then showed that the resulting dynamic equations can be expressed recursively for applications requiring computationally efficient dynamics algorithms, or can be cast into closed-form for applications requiring high-level manipulation of the equations of motion. Moreover, the dynamic equations are formulated in a completely coordinate-invariant manner, and as a result are not bound to any specific set of local link reference frames in which to express the kinematic and dynamic parameters of the robot.

References

[1] C. A. Balafoutis and R. V. Patel, *Dynamic Analysis of Robotic Manipulators: A Cartesian Tensor Approach*. Boston, MA: Kluwer, 1991.

[2] B. A. Dubrovin, A. T. Fomenko, and S. P. Novikov, *Modern Geometry: Methods and Applications, Part 1*. New York: Springer-Verlag, 1984.

[3] R. Featherstone, *Robot Dynamics Algorithms*. Boston, MA: Kluwer, 1987.

[4] O. Khatib, "A unified approach for motion and force control of robot manipulators: The operational space formulation," *IEEE Robot. Automat.*, vol. RA-3, pp. 43–53, Feb. 1987.

[5] J. Y. S. Luh, M. H. Walker, and R. P. Paul, "On-line computational scheme for mechanical manipulators," *ASME J. Dyn. Syst., Meas., Contr.*, vol. 102, pp. 69–76, 1980.

[6] B. J. . Martin and J. E. Bobrow, "Minimum-effort motions for open-chain manipulators with task-dependent end-effector constraints," *Int. J. Robot. Res.*, vol. 18, no. 2, pp. 213–224, 1999.

[7] R. M. Murray, Z. Li, and S. S. Sastry, *A Mathematical Introduction to Robot Manipulation*. Boca Raton, FL: CRC, 1993.

[8] F. C. Park, J. E. Bobrow, and S. R. Ploen, "A Lie group formulation of robot dynamics," *Int. J. Robot. Res.*, vol. 14, no. 6, pp. 609–618, 1995.

[9] S. R. Ploen, *Geometric Algorithms for the Dynamics and Control of Multibody Systems*, Ph.D. dissertation, Univ. California, Irvine, 1997, http://www.eng.uci.edu/~sploen/srpindex.html.

[10] S. R. Ploen, J. E. Bobrow, and F. C. Park, "Geometric algorithms for operational space dynamics and control," in *Proc. IEEE Int. Conf. Robot. Automat.*, Albuquerque, NM, 1997, pp. 1606–1611.

[11] G. Rodriguez, A. Jain, and K. Kreutz-Delgado, "A spatial operator algebra for manipulator modeling and control," *Int. J. Robot. Res.*, vol. 10, no. 4, pp. 371–381, 1991.

[12] ——, "Spatial operator algebra for multibody system dynamics," *J. Astronaut. Sci.*, vol. 40, no. 1, pp. 27–50, 1992.

[13] G. Rodriguez and K. Kreutz-Delgado, "Spatial operator factorization and inversion of the manipulator mass matrix," *IEEE Trans. Robot. Automat.*, vol. 8, pp. 65–76, Feb. 1992.

[14] W. M. Silver, "On the equivalence of Lagrangian and Newton-Euler dynamics for manipulators," *Int. J. Robot. Res.*, vol. 1, no. 2, pp. 118–128, 1982.

A Vision-Based Method for the Circle Pose Determination With a Direct Geometric Interpretation

Zen Chen and Jen-Bin Huang

***Abstract*— A novel vision-based method for the circle pose determination is addressed. This method is based on two particular projected chords of a circle image. The first one is the projection of a circle chord which subtends the largest apex angle of the viewing cone for the circle image and the second one is the projection of a circle diameter whose backprojection plane bisects the above largest apex angle. This method is conceptually simple, since the circle center is the center point of the diameter chord and the circle orientation is given by the cross product of these two (directed) chords. We present theorems on the geometry of both the viewing cone and a reprojected circle image which are essential to the pose determination. We then give a pose determination method which is applicable under all viewing conditions. Experimental results illustrate the good performance of the method, when compared with other existing methods.**

***Index Terms*—Circular feature, elliptical image, largest apex angle, pose determination, principal axes, viewing cone.**

Manuscript received July 16, 1997; revised May 25, 1999. This paper was recommended for publication by Associate Editor T. Henderson and Editor V. Lumelsky upon evaluation of the reviewers' comments.

The authors are with the Department of Computer Science and Information Engineering, National Chiao Tung University, Hsinchu, Taiwan 30050, R.O.C. (e-mail: zchen@csie.nctu.edu.tw).

Publisher Item Identifier S 1042-296X(99)09234-4.

I. Introduction

The circular feature is a popular feature of industrial or man-made products. Therefore, estimating the three-dimensional (3-D) location and orientation of a circle with a known radius from its single perspective image is of fundamental importance. The major and minor axes of the ellipse are generally not the projections of any diameter of the circular object. In addition, the ellipse center is not the projection of the circle center, so the explicit geometric relations between two-dimensional (2-D) image feature points and the 3-D object pose parameters are not readily available. Thus, man-made marking feature such as the circle center [1] or a diameter [2] was utilized in order to set up the equations needed in solving the object pose problem. On the other hand, there are approximation methods [2]–[3] that make simplifying assumptions to convert a complex problem to a simple one. For instance, an orthographic projection is used to replace the perspective projection, or the optical axis of the camera is assumed to pass through the center of the circular object. Recently, Safaee-Rad *et al.* [4] and Kanatani *et al.* [5] proposed exact methods for the circle pose estimation without using any marking feature or simplifying assumptions. These two methods are basically the same in terms of their problem formulations using the matrix form. In these two methods no explicit geometric relations between 2-D image feature points and the 3-D object pose parameters were employed. So, these methods are more or less an algebraic method which has no intuitive geometric interpretation. Besides, these methods break down when the viewing cone becomes degenerate, because no ellipse can be fitted to the line-shaped image.

We shall present a novel vision-based method for the circle pose determination. The circle pose parameters (i.e., circle center and circle orientation) are obtained directly through the determination of the 3-D positions of two particular chords of the circle from the circle image. To begin with, it is observed that a fixed viewing cone is formed jointly by the camera lens center G and the projected circle contour in the image plane. One chord (or its projected chord) is defined to be the one which subtends the largest apex angle at the apex G of the viewing cone. The other chord (or its projected chord) is defined so that its backprojected plane contains the bisector of the largest apex angle. We present theorems on the viewing geometry which are essential to the pose determination. Finally, we give a pose determination procedure which yields the closed form and exact solution(s). The method is applicable under all viewing conditions including

1) right viewing cone;
2) elliptical viewing cone;
3) degenerate viewing cone.

And, it has a clear geometric interpretation.

The rest of this paper is organized as follows. Section II introduces the largest apex angle and the two particular chords. The important theorems on the viewing geometry are derived. Section III sets up the geometric equations to find the 3-D positions of endpoints of the two chords and their middle points. The closed-form solutions to the pose parameters of the circle are then given. Section IV presents the experimental results of the application of the method to the real images. Section V is the conclusion.

II. The Geometric Model for Object Pose Determination

The general perspective projection of a circle (i.e., a circular object) is an ellipse. However, the general perspective projection becomes circular if the camera optical axis is rotated such that it is perpendicular to the supporting plane of the circular object. When the camera lens center incidentally lies on the supporting plane of the circular object, the perspective projection degenerates to a line segment. A viewing cone is depicted in Fig. 1. Here the apex of the viewing cone is the camera lens center G, and the perspective projection of the circular object is denoted by E. It will be shown that there exists an apex angle of the viewing cone which is the largest, called the ***largest apex angle*** (LAA). Let the chord of the ellipse E subtending the angle LAA be chord $\overline{pq}$ and let its corresponding chord on the circular object be chord $\overline{PQ}$. Next, denote the supporting plane containing the apex G and chord $\overline{pq}$ (or $\overline{PQ}$) as plane $P_{\rm LAA}$. The unit vector along the bisector of the angle LAA can be found to be $\vec{w} \equiv (\overrightarrow{u_{Gp}} + \overrightarrow{u_{Gq}})/|\overrightarrow{u_{Gp}} + \overrightarrow{u_{Gq}}|$, where $\overrightarrow{u_{Gp}}$ and $\overrightarrow{u_{Gq}}$ are the unit vector of the vectors $\overrightarrow{Gp}$ and $\overrightarrow{Gq}$, respectively. The unit vector denoting the orientation of plane $P_{\rm LAA}$ is given by $\vec{v} \equiv (\overrightarrow{u_{Gp}} \times \overrightarrow{u_{Gq}})/|\overrightarrow{u_{Gp}} \times \overrightarrow{u_{Gq}}|$. Furthermore, the plane which is perpendicular to the plane $P_{\rm LAA}$ and passes through the bisector of the angle LAA is denoted by $P^{\perp}_{\rm LAA}$. It can be readily shown that the normal vector of the plane $P^{\perp}_{\rm LAA}$ is given by $\vec{u} = \vec{w} \times \vec{v}$. Assume that plane $P^{\perp}_{\rm LAA}$ intersects the ellipse E and the circular object on chords $\overline{bc}$ and $\overline{BC}$, respectively. Also, let the bisector of the angle LAA intersect the image plane at point m and the circular object at point M. Now, imagine that the camera optical axis is rotated such that the new optical axis, the Z'-axis, is in the direction of $\vec{w}$ defined above. Also let the new x'- and y'-axes be so arranged that they are respectively in the directions of $\vec{u}$ and $\vec{v}$. Then, the perspective projection of the circular object on the image plane specified by $Z' = f$ (f is the effective focal length) is a new ellipse, called E'. (Actually we do not need to physically construct the ellipse E'; it is a conceptual ellipse). Notice that the viewing cone associated with the new ellipse E' is the same as before, since the camera lens center and the circle remain the same. Assume the new intersection points between optical rays $\overrightarrow{Gp}$, $\overrightarrow{Gq}$, $\overrightarrow{Gb}$, $\overrightarrow{Gc}$, $\overrightarrow{Gm}$, and ellipse E' are denoted by points p', q', b', c', and m', respectively (refer to Fig. 3). We shall show the conditions for existence and uniqueness of the angle LAA and the geometric properties of the new ellipse E'. These results will be used in the object pose determination.

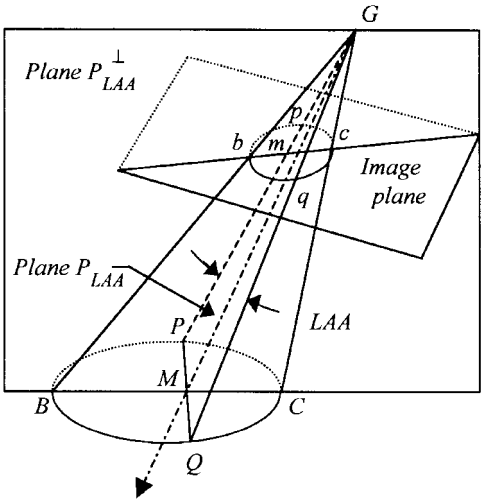

Fig. 1. Viewing geometry of a circular object.

In the following it is assumed that the distance between the apex of the viewing cone and the closest circular object point is

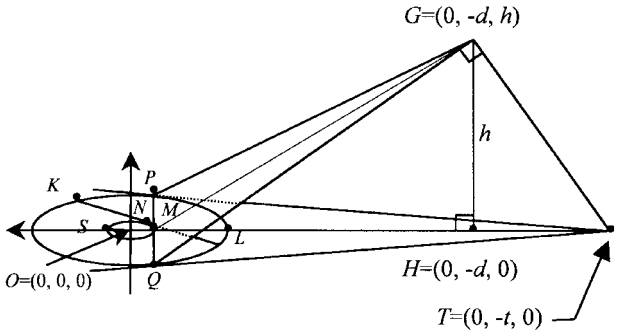

Fig. 2. Apex angle subtended by a chord of the circular object and the relevant geometric entities.

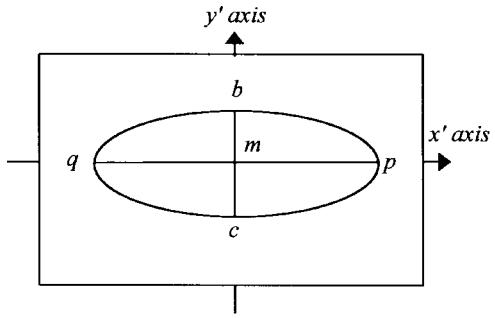

Fig. 3. Principal axes of ellipse E'.

larger than the object radius. This assumption holds in the practical applications. Furthermore, in Theorem 1 the viewing cone is assumed to be an elliptical cone, not a circular cone. That is, the camera lens is not right above the circular object center. The circular cone will be shown as a special case. We shall also refer to the family of all chords of the circular object which have an identical length L as a set denoted by $\{\text{Chords } (L)\}$ and the family of the apex angles subtended by the chords in $\{\text{Chords } (L)\}$ as the set $\{\text{Apex-Angles-Opposite-To-Chords } (L)\}$. In Fig. 2, a perpendicular line, $\overline{GH}$ is constructed from the cone apex G to the circular object plane, where point H is the intersection point on the object plane. The middle points of the chords in the set $\{\text{Chords } (2l)\}$ form a concentric circle centered at the circular object center O. The line $\overline{HO}$ generally intersects the concentric circle at two points, denoted by M and S. Let the chord tangent to the concentric circle at point M be denoted by chord $\overline{PQ}$. Then, $\overline{PQ}$ is perpendicular to line $\overline{HO}$ and point M is the middle point of $\overline{PQ}$. In addition, $\overline{PQ}$ is perpendicular to the line connecting points G and M. Furthermore, point M is closest to both points H and G among all the middle points of chords in the set $\{\text{Chords } (2l)\}$ and M is unique, if the viewing cone is a general elliptical cone.

Theorem 1 In a general elliptical viewing cone a chord in the set $\{\text{Chords } (2l)\}$ subtends the largest apex angle in the set $\{\text{Apex-Angles-Opposite-To-Chords } (2l)\}$, if and only if the following conditions hold:

1) the chord is perpendicular to the line connecting the chord middle point and the cone apex;
2) the chord middle point has the shortest distance to the cone apex among all middle points of chords in the set $\{\text{Chords } (2l)\}$.

Proof: (a) To show the "if" part:

Assume a chord $\overline{PQ}$ satisfies conditions 1) and 2). If the chord $\overline{PQ}$ does not subtend the largest apex angle, then there must exist another chord, denoted as chord $\overline{KL}$, which subtends the largest apex angle $\angle KGL$. Denote the middle points of chords $\overline{KL}$ and $\overline{PQ}$ as points N and M, respectively. Since point M is the unique point which has the shortest distance to the cone apex G among all the middle points, so $|\overline{GM}| < |\overline{GN}|$. To compare the magnitudes of angles $\angle KGL$ and $\angle PGQ$, we overlap the supporting plane of the angle $\angle PGQ$ with that of the angle $\angle KGL$ such that points M and N coincide. Since line $\overline{MG} < \overline{NG}$, the two lines no longer meet at point G, after we overlap the other two endpoints M and N. We redenote $\overline{MG}$ by $\overline{MG_1}$ and $\overline{NG}$ by $\overline{NG_2}$. The coordinates of the above points can be assigned as $M = N = (0,0)$, $G_1 = (0,e)$, $G_2 = (0,e')$, $P = (l,0)$, $Q = (-l,0)$, $K = (l\cos\theta, l\sin\theta)$, and $L = (-l\cos\theta, -l\sin\theta)$, where θ is the angle between $\overline{KL}$ and $\overline{PQ}$ and $l > 0$, $e' > e > 0$. Then

$$\cos(\angle PG_1Q) = (-l^2+e^2)/(l^2+e^2), \quad \text{and}$$
$$\cos(\angle KG_1L) = (-l^2+e^2)/\sqrt{(l^2+e^2)^2 - 4le\sin^2\theta}.$$

Here, e is the distance from the apex G (i.e., G_1) to the circular object point M. By assumption, $e' > e > R \geq l$, so $\cos(\angle KG_2L) > \cos(\angle KG_1L) \geq \cos(\angle PG_1Q)$. Thus $\angle KG_2L < \angle PG_1Q$. This is contradictory to the assumption that $\angle KGL$ is the largest apex angle. Therefore, $\angle PGQ$ must be the largest apex angle.

(b) To show the "only if" part:

Assume the chord $\overline{IJ}$ subtends the largest apex angle. If the chord $\overline{IJ}$ does not satisfy conditions 1) or 2), then we shall show there is a contrasiction.

Case (i): If condition 1) is not satisfied by the chord $\overline{IJ}$, then there exists a chord $\overline{PQ}$ which satisfies condition 1). Using the same reasoning as in part (a) except that $\overline{KL}$ is replaced by $\overline{IJ}$, we can show that the apex angle subtended by chord $\overline{IJ}$ is smaller than that subtended by chord $\overline{PQ}$. This is a contradiction. Therefore, condition 1) must be satisfied.

Case (ii): If condition 2) is not satisfied by chord $\overline{IJ}$, then there exists a chord $\overline{PQ}$ whose middle point has the shortest distance to the cone apex G among all middle points of chords in the set $\{\text{Chords } (2l)\}$. Again, it can be shown that the apex angle subtended by chord $\overline{IJ}$ is smaller than that subtended by chord $\overline{PQ}$. This is a contradiction. Therefore, condition 2) must be satisfied. This completes the proof. □

Theorem 2 If the viewing cone is a right circular cone, the largest apex angle (LAA) is not unique and can be subtended by any diameter of the circular object. Otherwise, the angle LAA is unique and is not subtended by any diameter of the circular object.

Proof: (a) If the viewing cone is a right circular cone, then the apex angles subtended by all diameters are equally large and they are larger than that subtended by any nondiameter chord. Therefore, the angle LAA is not unique and can be subtended by any diameter of the circular object.

(b) If the viewing cone is not a right circular cone, namely, it is a general elliptical cone. According to Theorem 1, if the chord $\overline{PQ}$ subtends the largest apex angle among the chords of a certain length, then the line $\overline{MG}$ connecting the middle point M of $\overline{PQ}$ and the apex G is perpendicular to $\overline{PQ}$. In the 3-D object-centered coordinate system, as shown in Fig. 2, we can assume $O = (0,0,0)$, $M = (0,-v_M,0)$, $P = (\sqrt{R^2 - v_M^2}, -v_M, 0)$, $Q = (-\sqrt{R^2 - v_M^2}, -v_M, 0)$, and $G = (0,-d,h)$, where $d \geq 0$, $v_M \geq 0$, and $h > 0$. Then $\overrightarrow{GP} = (\sqrt{R^2 - v_M^2}, -v_M + d, -h)$ and $\overrightarrow{GQ} = (-\sqrt{R^2 - v_M^2}, -v_M + d, -h)$. The apex angle subtended by the chord $\overline{PQ}$ can be determined from $\cos(\angle PGQ) = \overrightarrow{GP} \cdot \overrightarrow{GQ}/(|\overrightarrow{GP}||\overrightarrow{GQ}|) = (2v_M^2 - 2dv_M + d^2 + h^2 - R^2)/(-2dv_M + d^2 + h^2 + R^2)$. For the given R, d, and h, the value of v_M which maximizes the apex angle $\angle PGQ$ is given by $\partial\cos(\angle PGQ)/\partial v_M = 0$.

Here $d \neq 0$, because if $d = 0$, the viewing cone is a right circular cone. Thus $v_M = (d^2 + h^2 + R^2)/2d \pm \sqrt{((d^2 + h^2 + R^2)/(2d))^2 - R^2}$. Since $(d^2 + h^2 + R^2)/2d \geq R$ and $0 \leq v_M \leq R$, there is only one solution of v_M, i.e.,

$$v_M = v_M = (d^2+h^2+R^2)/2d - \sqrt{((d^2 + h^2 + R^2)/(2d))^2 - R^3}.$$

Because $v_M \neq 0$, $\overline{PQ}$ is not a diameter of the circular object. □

Theorem 3 Let the optical axis of the camera be realigned with the bisector of the angle LAA, then the intersection line between the ellipse E' and the plane $P_{\mathrm{LAA}}^{\perp}$ is a principal axis of E'.

Proof: The plane $P_{\mathrm{LAA}}^{\perp}$ passes through the circle center of the circular object, O. Therefore, the plane $P_{\mathrm{LAA}}^{\perp}$ cuts the circular object into two symmetrical halves. And the two symmetric halves of the circular object are evenly projected onto the new image plane with line $\overline{GM}$ being the camera optical axis. Therefore, the intersection line between the ellipse E' and the plane $P_{\mathrm{LAA}}^{\perp}$ is a principal axis of E' by definition. □

Theorem 4 The intersection line between the ellipse E' and the plane P_{LAA} is the second principal axis of ellipse E'.

Proof: The intersection line between the ellipse E' and the plane P_{LAA}, denoted by the line $\overline{p'q'}$, is the projection of the chord $\overline{PQ}$ of the circular object that subtends the angle LAA.

Case (1): If the viewing cone is a right cone, by Theorem 2, the chord $\overline{PQ}$ subtending the largest apex angle is a circle diameter. The ellipse E' becomes circular and the perspective projection of $\overline{PQ}$ is a diameter of the circular ellipse E'. Therefore, it is a principal axis of E'.

Case (2): If the viewing cone is not a right cone, the chord $\overline{PQ}$ subtending the angle LAA is not a diameter of the circular object by Theorem 2. We shall show below that the projection of the chord $\overline{PQ}$, $\overline{p'q'}$, is the longest chord of E' perpendicular to the first principal axis $\overline{b'c'}$ of E' stated in Theorem 3. That is, $\overline{p'q'}$ is the second principal axis of E'.

First of all, planes P_{LAA} and $P_{\mathrm{LAA}}^{\perp}$ are perpendicular to each other. Since their intersection line which is the bisector of the angle LAA is the optical axis for the elliptical image E'. The projected line of any line on plane P_{LAA} including $\overline{PQ}$ is perpendicular to the projected line of any line on plane $P_{\mathrm{LAA}}^{\perp}$ including $\overline{BC}$. That is, the chord $\overline{p'q'}$ is perpendicular to the first principal axis $\overline{b'c'}$ of the elliptical image E'.

Next, let lines $\overline{PT}$ and $\overline{QT}$ be two tangent lines to the circular object at points P and Q, where point T is the intersection point of these two tangent lines, as shown in Fig. 2. The projection of the tangent line $\overline{PT}$ on the elliptical image E' is a tangent line of E' at point p', denoted by line l_1 (refer to Fig. 3). Similarly, the projection of the tangent line $\overline{QT}$ on E' is another tangent line of E' at point q', denoted by l_2. To show the chord $\overline{p'q'}$ has the longest length among all the chords perpendicular to the principal axis $\overline{b'c'}$ is equivalent to showing that lines l_1 and l_2 are parallel. As in the proof of Theorem 2, on the 2-D circular object's supporting plane, point O is denoted as the origin $(0,0)$, and the middle point M of the chord $\overline{PQ}$ has the coordinates $(0,-v_M)$, where

$$v_M = v_M = (d^2+h^2+R^2)/2d - \sqrt{((d^2 + h^2 + R^2)/(2d))^2 - R^2}.$$

Also, the coordinates of point P are $(\sqrt{R^2 - v_M^2}, -v_M)$. Let the coordinates of point T be $(0,-t)$. Since $\overrightarrow{PO} \cdot \overrightarrow{PT} = 0$, so $(\sqrt{R^2 - v_M^2})^2 + v_M(v_M - t) = 0$. It yields $t = R^2/v_M$. Now, in the 3-D object-centered space, $O = (0,0,0)$, $M = (0,-v_M,0)$, $G = (0,-d,h)$, $P = (\sqrt{R^2 - v_M^2}, -v_M, 0)$, $Q = (-\sqrt{R^2 - v_M^2}, -v_M, 0)$, and $T = (0,-t,0)$. So

$$\overline{GM} \cdot \overline{GT} = d^2 - (v_M + R^2/v_M)d + R^2 + h^2.$$

After substituting the value of v_M into the equation, $\overrightarrow{GM} \cdot \overrightarrow{GT} = 0$. Therefore, the line $\overline{GT}$ is parallel to the image plane. Next, to show that the tangent lines l_1 and l_2 are parallel: assume lines l_1 and l_2 intersect, then their intersection point must lie on the common line of planes PGT and QGT which is the line $\overline{GT}$. However, the line $\overline{GT}$ is parallel to the image plane on which lines l_1 and l_2 lie, so it is contradictory to the assumption that lines l_1 and l_2 intersect on line $\overline{GT}$. Thus, lines l_1 and l_2 must be parallel. This completes the proof of the theorem. □

III. Circle Pose Estimation Based on Spatial Relations Between 2-D and 3-D Feature Points

Based on Theorem 4, it is easy to find that the chord $\overline{p'q'}$ subtending the largest apex angle is the major axis of the new elliptical image E'. On the other hand, the chord $\overline{b'c'}$ is the minor axis of E' (see Fig. 3). Thus, in the camera coordinate system the 2-D feature points of the two principal axes of ellipse E' are $b' = (0, v_{b'}, f)$, $c' = (0, -v_{c'}, f)$, $p' = (u_{p'}, 0, f)$, and $q' = (-u_{q'}, 0, f)$, where $v_{b'} = v_{c'} = f\tan(\angle b'Gc'/2)$ and $u_{p'} = u_{q'} = f\tan(\angle p'Gq'/2)$. Based on the geometric properties of the viewing cone, the 3-D feature points on the circle can be specified as $B = \alpha b' = (0, \alpha v_{b'}, \alpha f)$, $C = \beta c' = (0, -\beta v_{c'}, \beta f)$, $P = \gamma p' = (\gamma u_{p'}, 0, \gamma f)$, $Q = \gamma q' = (-\gamma u_{q'}, 0, \gamma f)$, and $M = (P+Q)/2 = (0,0,\gamma f)$. Also, $O = (B+C)/2 = (0, v_{b'}(\alpha-\beta)/2, (\alpha+\beta)f/2)$, and $G = (0,0,0)$.

To find the coordinates of the above 3-D feature points, we need three equations for the three unknowns α, β, and γ which are given by (a) $|\overline{OB}| = |\overline{OC}| = R$; (b) $|\overline{OP}| = |\overline{OQ}| = R$; (c) and $|\overline{GB}|/|\overline{GC}| = |\overline{BM}|/|\overline{CM}|$ where R is the given radius.

The first two equations are obtained from the properties of the circle and the third equation is stated in the following theorem.

Theorem 5 The lengths of $\overline{GB}$, $\overline{GC}$, $\overline{BM}$, and $\overline{CM}$ are related by

$$|\overline{GB}|/|\overline{GC}| = |\overline{BM}|/|\overline{CM}|.$$

Proof: Consider the triangle $\triangle BGC$. Line $\overline{GM}$ (or $\overline{Gm'}$) is the bisector of $\angle BGC$ (or $\angle b'Gc'$). Obviously, the distance from point M to line $\overline{GB}$ is equal to that from point M to line $\overline{GC}$. Denote this distance as h_1. Also denote the distance from point G to line $\overline{BC}$ as h_2. Then, $\mathrm{Area}(\Delta BGM) = |\overline{GB}|h_1/2 = |\overline{BM}|h_2/2$, and $\mathrm{Area}(\Delta CGM) = |\overline{GC}|h_1/2 = |\overline{CM}|h_2/2$. Thus $|\overline{GB}|/|\overline{GC}| = |\overline{BM}|/|\overline{CM}|$. □

We can rewrite (a)–(c), in terms of α, β, and γ, as $(\alpha+\beta)^2 v_{b'}^2 + (\alpha-\beta)^2 f^2 = 4R^2$, $4\gamma^2 u_{p'}^2 + (\beta-\alpha)^2 v_{b'}^2 + (2\gamma-\alpha-\beta)^2 f^2 = 4R^2$, and $\gamma = 2\alpha\beta/(\alpha+\beta)$. By eliminating γ and after some rearranging, we obtain $\alpha+\beta = \pm 2R\sqrt{(u_{p'}^2 + f^2)/(v_{b'}^2 + f^2)}/u_{p'}$ and $\alpha - \beta = \pm 2R\sqrt{(u_{p'}^2 - f^2)/(v_{b'}^2 + f^2)}/u_{p'}$. Since $\alpha+\beta > 0$, the negative value of $\alpha+\beta$ is discarded. From these equations, there are two final solutions for α, β, and γ:

$$\alpha_1 = R\Big(\sqrt{\big(u_{p'}^2 + f^2\big)/\big(v_{b'}^2 + f^2\big)} + \sqrt{\big(u_{p'}^2 - f^2\big)/\big(v_{b'}^2 + f^2\big)}\Big)/u_{p'},$$

$$\beta_1 = R\Big(\sqrt{\big(u_{p'}^2 + f^2\big)/\big(v_{b'}^2 + f^2\big)} - \sqrt{\big(u_{p'}^2 - f^2\big)/\big(v_{b'}^2 + f^2\big)}\Big)/u_{p'},$$

$$\gamma_1 = 2\alpha_1\beta/(\alpha_1+\beta) = R\Big(\sqrt{\big(u_{p'}^2 + f^2\big)/\big(v_{b'}^2 + f^2\big)}\Big)/u_{p'}.$$

And

$$\alpha_2 = \beta_1, \quad \beta_2 = \alpha_1, \quad \gamma_2 = \gamma_1.$$

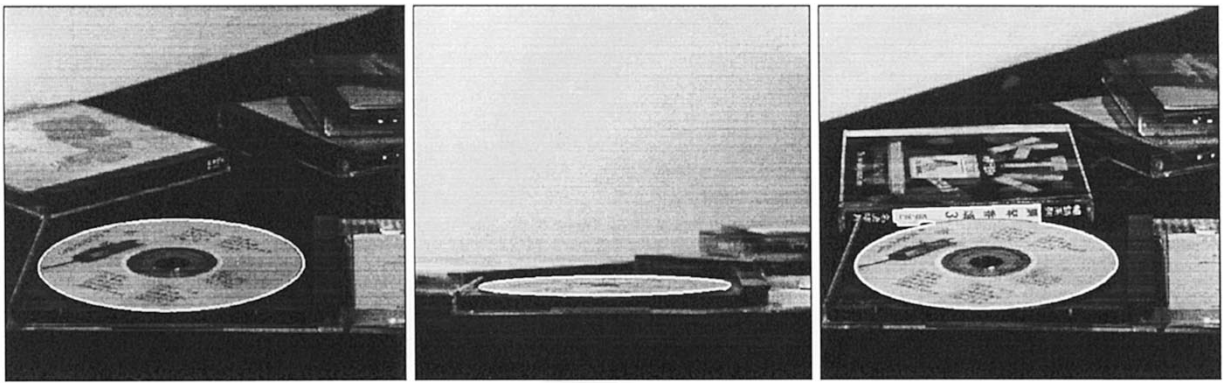

(a) (b) (c)

Fig. 4. (a)–(c) Three different images of a CD. The contour of the CD found in each image is marked in white color.

TABLE I
THE COMPARISON OF THE POSE PARAMETERS OBTAINED BY THREE DIFFERENT METHODS FOR A CD

Method	Image type	Circle center position of the circle	Position Difference (mm)	Surface normal of the circle	Orientation Difference (deg)
Our method	(a)	(-14.86, 31.54, 902.38)	--	(-0.00, -0.97, -0.24)	--
	(b)	(-3.58, 41.95, 935.47)		(-0.01, -1.00, -0.02)	
	(c)	(-14.86, 31.54, 902.38)		(-0.01, -0.97, -0.24)	
K and L's method	(a)	(-14.91, 31.66, 902.46)	0.15	(-0.01, -0.97, -0.25)	0.43
	(b)	(-3.53, 41.16, 916.66)	18.83	(-0.01, -1.00, -0.02)	0.15
	(c)	(-18.61, 28.88, 919.65)	17.87	(0.02, -0.95, -0.31)	4.15
K and A's method	(a)	(-14.44, 31.57, 872.42)	29.96	(-0.01, -0.96, -0.28)	2.45
	(b)	(-3.42, 39.97, 886.66)	48.85	(-0.01, -1.00, -0.07)	2.68
	(c)	(-18.05, 29.05, 888.96)	14.02	(0.01, -0.94, -0.34)	5.88

After we obtain the 3-D feature points on the circle, we can readily compute the 3-D circle pose parameters as follows. First, the two solutions to the circle center O are given by

$$O_1 = \left(0, \frac{Rv_{b'}}{u_{p'}}\sqrt{\frac{u_{p'}^2 - v_{b'}^2}{v_{b'}^2 + f^2}}, \frac{Rf}{u_{p'}}\sqrt{\frac{u_{p'}^2 + f^2}{v_{b'}^2 + f^2}}\right) = (O_X, O_Y, O_Z) \quad \text{and} \quad O_2 = (O_X, -O_Y, O_Z)$$

Next, the two solutions to the circle orientation are given by

$$\overrightarrow{n_1} = \frac{\overline{PQ} \times \overline{BC}}{|\overline{PQ} \times \overline{BC}|} = \frac{\left(0, \sqrt{u_{p'}^2 - v_{b'}^2} f, -\sqrt{u_{p'}^2 + f^2} v_{b'}\right)}{\sqrt{\left(u_{p'}^2 - v_{b'}^2\right) f^2 + \left(u_{p'}^2 + f^2\right) v_{b'}^2}} = (n_X, n_Y, n_Z) \quad \text{and}$$

$$\overrightarrow{n_2} = (n_X, -n_Y, n_Z).$$

It is trivial to show that when the viewing cone is a right cone, $u_{p'} = v_{b'} = f\tan(\mathrm{LAA}/2) = fR/|\overline{GO}|$ and $\alpha_1 = \alpha_2 = \beta_1 = \beta_2 = \gamma_1 = \gamma_2 = R/u_{p'} = |\overline{GO}|/f$. Therefore, there is only one solution to the circle pose problem. On the other hand, when the viewing cone is degenerated as a line segment. $v_{b'} = 0$, $0 < u_{p'} < R$, $O_1 = O_2 = (0, 0, Rf\sqrt{1 + (u_{p'}/f)^2})/u_p$, $\overrightarrow{n_1} = (0, 1, 0)$, and $\overrightarrow{n_2} = (0, -1, 0)$. Therefore, there are two solutions, one with the surface facing up and the other one with the surface facing down.

IV. EXPERIMENTAL RESULTS

The experimental setup contains an ELMO SE320 CCD camera and a 512 × 480 frame grabber with a 8-bit resolution. The size of pixels is 0.01 mm. The camera aspect ratio is $1.212:1$; the effective focal length is 31.6 mm. The object is kept at a distance of about 1 m in the experiments. We shall compare three different methods for the circle pose determination:

1) our method (a geometric method);
2) Kanatani and Liu's method (an algebraic method);
3) Kabuka and Arenas' method (an approximation method).

Three input images of a CD are shown which correspond to a general view in Fig. 4(a), an elongated view in Fig. 4(b), and a view with an outlier (due to object touching) in Fig. 4(c). We obtain the contour map data for each image using a method based on the edge/border coincidence information described in [8]. In order to select the desired elliptical contour, the pre-specified length intervals of the two ellipse principal axes are used to examine the contour shape. The selected contours, which are marked in white color, are superimposed onto the original images. Due to the page limit, we cannot go through the details; one may refer to [9] for the details. After the contours are selected, the ellipse fitting program [6] was used to find the ellipse from the selected contour for the Kanatani and Liu's method. Our pose determination method and the other two exiting methods are applied to the elliptical contours extracted from each image. The experimental results of the three pose parameter estimation methods are listed in Table I. The position and surface orientation differences are calculated relative to our results. In the case of a general view, the estimation results obtained by our method and the Kanatani and Liu's method are roughly the same. This is so because both methods yielded the exact solutions. However, the Kabuka and Arenas' method yields a larger estimation error. This is due to the approximations made in the method. In the case of an elongated ellipse, the experimental result shows some differences among the methods. The error of the Kanatani and Liu's method is caused by the inaccuracy in the ellipse fitting. This confirms the finding in [7]; namely, an ellipse

fitting method generally has the effects of over- or under-estimated eccentricity of the fitted ellipse. Meanwhile, the Kabuka and Arenas' method, which are based on the lengths of the major and minor axes, yields the less accurate results again. In the case of a view with an outlier, the outlier causes the error in the ellipse fitting in the Kanatani and Liu's method and hampers their estimation accuracy. Nevertheless, our method still yields the same good result, since the outlier part is not used in our computing the 2-D and 3-D feature points.

We also test the sensitivity of our method against the noise due to the data acquisition and image processing error. The x and y coordinates of feature points are added with a Gaussian noise with zero mean and a standard deviation of 1, 2, or 3 pixels to simulate the effect of the noise on our method. Each perturbation simulation is repeated for 1000 times. For the given three Gaussian noise distributions the standard deviations of the circle center location and the surface orientation are 6.29, 12.91, and 18.63 mm and 1.63, 3.10, and 4.61 degrees, respectively. Therefore, the estimation method is fairly robust.

V. Conclusion

We describe a circle pose determination method which is directly based on two particular chords of the circular object. The corresponding 2-D feature chords can be defined through the use of two particular planes related to the 3-D viewing cone constructed from the image of the circular object. One plane is the supporting plane P_{LAA} of the largest apex angle of the viewing cone, and the other is the plane $P_{\mathrm{LAA}}^{\perp}$ which is perpendicular to plane P_{LAA} on the bisector of the largest apex angle. Based on the geometric properties of the 2-D and 3-D feature points of the circular object, we can derive the closed-form solution to the circle pose problem. The generality of the proposed method is also shown for all three types of viewing conditions. Experimental results on the real data illustrate a better performance of the method.

References

[1] M. H. Han and S. Rhee, "Camera calibration for three-dimensional measurement," *Pattern Recognit.*, vol. 25, no. 2, pp. 155–164, 1992.

[2] M. R. Kabuka and A. E. Arenas, "Position verification of a mobile robot using standard pattern," *IEEE Trans. Robot. Automat.*, vol. RA-3, pp. 505–516, Dec. 1987.

[3] B. Hussain and M. R. Kabuka, "Real-time system for accurate three-dimensional position determination and verification," *IEEE Trans. Robot. Automat.*, vol. 6, pp. 31–43, Feb. 1990.

[4] R. Safaee-Rad, I. Tchoukanov, K. C. Smith, and B. Benhabib, "Three-dimension of circular features for machine vision," *IEEE Trans. Robot. Automat.*, vol. 8,pp. 624–640, Oct. 1992.

[5] K. Kanatani and W. Liu, "3-D interpretation of conics and othogonality," *Comput., Vis., Graph., Image Process: Image Understand.*, vol. 58, no. 3, pp. 286–301, 1993.

[6] R. M. Haralick and L. G. Shapiro, *Computer and Robort Vision*. New York: Addison-Wesley, 1992.

[7] P. L. Rosin, "A note on the least squares fitting of ellipses," *Pattern Recognit. Lett.*, vol. 14, Oct. 1993.

[8] A. Rosenfeld and A. C. Kak, *Digital Picture Processing*, 2nd ed. New York: Academic, 1982, vol. II, pp. 127–129.

[9] Z. Chen and J. B. Huang, "Determination of 3-D orientation and location of a circular feature," Tech. Rep., Dept. Comput. Sci. Inform. Eng., Nat. Chiao Tung Univ., Hsinchu, Taiwan, R.O.C., 1998.

A Technique for Analyzing Constrained Rigid-Body Systems, and its Application to the Constraint Force Algorithm

Roy Featherstone and Amir Fijany

***Abstract*— The constraint force algorithm, as originally described by Fijany *et al.*, calculates the forward dynamics of a system comprising N rigid bodies connected together in an unbranched chain with joints from a restricted class of joint types. It was designed for parallel calculation of the dynamics, and achieves $O(\log N)$ time complexity on $O(N)$ processors. This paper presents a new formulation of the Constraint Force Algorithm that corrects a major limitation in the original, and sheds new light on the relationship between it and other dynamics algorithms. The new version is applicable to systems with any type of joint, floating bases, and short branches off the main chain. It is obtained using a new technique for analysing constrained rigid-body systems by means of a change of basis in a dual system of vector spaces. This new technique is also described.**

***Index Terms*—Constrained dynamics, dual vector space, robot dynamics algorithm.**

I. Introduction

THE constraint force algorithm (CFA) was the first algorithm to calculate the forward dynamics of an N-body robot manipulator in $O(\log N)$ time on a parallel computer with $O(N)$ processors. The original version, as described in [1], was applicable to a system comprising a fixed base and N rigid bodies, connected together in an unbranched chain by joints from a restricted class of joint types. This was subsequently extended to floating bases in [2].

This paper presents a new formulation of the CFA that corrects a major limitation in the original formulation, and sheds new light on the relationship between the CFA and other dynamics algorithms. It also presents an improved method for dealing with floating bases that is easier and more efficient than the method described in [2]; and it extends the CFA to branched kinematic trees consisting of a single main chain and any number of short side-branches. Floating bases are implemented by means of a 6-DoF joint, and short branches are implemented using articulated-body techniques.

The original formulation, as described in [1], includes an incorrect usage of orthogonal complements. Specifically, the inner product that is used to define orthogonality is noninvariant and dimensionally inconsistent. See [3] for a full explanation of the problem. In [1], the problem is finessed by observing that if the algorithm is restricted to certain types of joint then it is possible to formulate the affected (6) and (7) in such a way that the coefficients of the dimensionally-inconsistent terms are zero. The new formulation removes the source of the problem by avoiding orthogonal complements altogether. The immediate result is to remove all restrictions on joint type.

Manuscript received July 27, 1998; revised August 11, 1999. This paper was recommended for publication by Associate Editor W. Wilson and Editor A. De Luca upon evaluation of the reviewers' comments. This work was supported in part by EPSRC Advanced Research Fellowship B92/AF/1466 and the National Aeronautics and Space Administration.

R. Featherstone was with the Department of Engineering Science, Oxford University, Oxford, U.K. He is now with the Department of Computer Science, University of Wales Aberystwyth, Penglais, Aberystwyth SY23 3DB, U.K.

A. Fijany is with the Jet Propulsion Laboratory, California Institute of Technology, Pasadena, CA 91109 USA.

Publisher Item Identifier S 1042-296X(99)10389-6.